High-resolution measurement, line identification, and spectral modeling of the $K\beta$ spectrum of heliumlike argon emitted by a laser-produced plasma using a gas-puff target

Igor Yu. Skobelev, Anatoly Ya. Faenov, and Vladimir M. Dyakin
Multicharged Ion Spectra Data Center, VNIIFTRI, Mendeleevo, 141570 Russia

Henryk Fiedorowicz, Andrzej Bartnik, and Miroslaw Szczurek
Institute of Optoelectronics, Military University of Technology, 01-489 Warsaw, Poland

Peter Beiersdorfer, Joseph Nilsen, and Albert L. Osterheld
Lawrence Livermore National Laboratory, Livermore, California 94551
(Received 9 August 1996; revised manuscript received 4 November 1996)

We present an analysis of the spectrum of satellite transitions to the He-β line in Ar XVII. High-resolution measurements of the spectra from laser-heated Ar-gas-puff targets are made with spectral resolution of 10 000 and spatial resolution of better than 50 μm. These are compared with tokamak measurements. Several different lines are identified in the spectra and the spectral analysis is used to determine the plasma parameters in the gas-puff laser-produced plasma. The data complement those from tokamak measurements to provide more complete information on the satellite spectra. [S1063-651X(97)05803-0]

PACS number(s): 52.70.La, 32.30.Rj, 32.70.−n

Electron temperatures of 500–1000 eV are routinely achieved in laboratory plasma sources such as laser-produced plasmas, fast pinches, and tokamaks. As a result, mid-Z elements are typically found in the heliumlike charge state and radiate in the x-ray region. The heliumlike $K\alpha$ emission consisting of transitions from the $n=2$ levels to $n=1$ has been studied in detail in both tokamak and laser-produced plasmas [1,2]. These studies have demonstrated the great utility of the $K\alpha$ spectra for determining various plasma parameters such as the electron and ion temperatures, the plasma density, the ion transport coefficients, and the fraction of non-Maxwellian electrons.

K-shell x-ray spectra involving transitions from levels higher than $n=2$ have been studied in much less detail. We believe such K-shell spectra ($K\beta$, $K\gamma$, etc.) in many cases could be even more useful for diagnostic applications than the traditionally used $K\alpha$ emission, because these transitions, as a rule, are optically thin even in a dense laser-produced plasma. The most detailed investigations of the heliumlike argon $K\beta$ spectra have been made recently on the Princeton Large Torus tokamak [3] and on the Livermore electron-beam ion trap (EBIT) facility [4]. In the present paper these spectra have been investigated for the case of a high-density laser-produced plasma. Using this type of plasma source it is possible to test the atomic theory for a plasma that is in an intermediate regime between that described by coronal (collisionless) and local thermodynamic equilibrium approximations. Our measurements include the positions and strengths of the $1s2l3l'$-$1s^2 2l$ and $1s2l4l'$-$1s^2 2l$ lithiumlike satellite lines, $K\beta_1$ and $K\beta_2$ heliumlike lines, and $1s^2 5d$-$1s^2 2p$ lithiumlike transitions. A detailed comparison of the measured argon spectrum with the theoretical data has been made. Good agreement is obtained for both the wavelengths and the intensities of the spectral lines, which allows us to estimate the parameters of the laser-produced plasma from the gas-puff target.

The experiments were carried out at the Institute of Optoelectronics, Poland. To heat the plasma, a Nd laser with pulse energy of 5–10 J and pulse duration of 1 nsec was focused to a 150-μm spot. An argon-gas-puff target was created by pulsed injection of gas from a high-pressure electromagnetic value through a 0.5-mm-diam nozzle into the vacuum. The gas backing pressure in the valve was 15 atm. The time delay between the laser pulse and the opening of the valve could be changed from 0.25 to 1 msec. The laser beam was focused onto the gas-puff target perpendicular to the flow of the gas and intersected the axis of the nozzle. By changing the time delay and the distance between the center of the laser spot and the output of the nozzle we could vary the gas pressure in the laser interaction region.

An x-ray pinhole camera was used for obtaining a qualitative description of the interaction of the laser radiation with the dense Ar gas. A typical pinhole image is shown in Fig. 1(a). In the pinhole image we see a small hot region near the line focus and a much larger, expanded region, which is much colder and less ionized than the small region near line

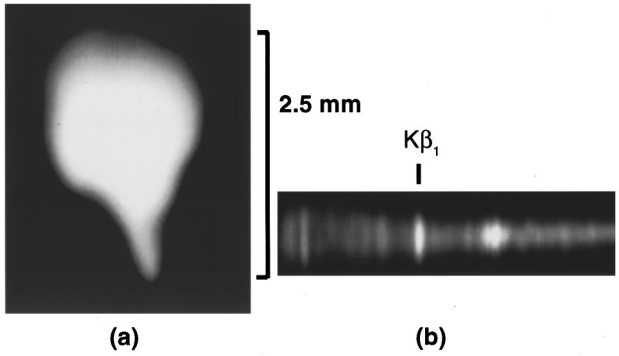

FIG. 1. (a) Typical x-ray pinhole image of the Ar-gas-puff laser-produced plasma and (b) plasma emission spectrum in the wavelength region 3.25–3.45 Å.

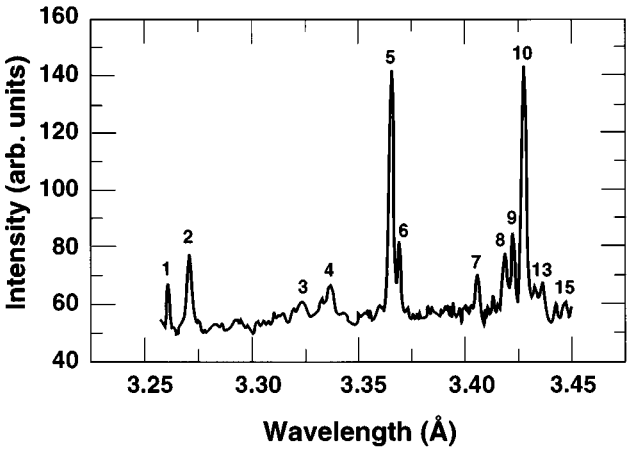

FIG. 2. Emission spectrum of the Ar-gas-puff laser-produced plasma in the wavelength region 3.25–3.45 Å taken with the FSSR 1D spectrometer.

focus that is emitting the x rays. Quantitative information on the x-ray plasma emission was obtained with the help of the FSSR (focusing spectrograph with spatial resolution) one-dimensional (1D) spectrometer [5]. This spectrometer employed a mica crystal with a lattice spacing (for fifth order of reflection) $d_5=9.722\ 05$ Å, which was spherically bent to a radius $R=100$ mm. The resolving power of the instrument was about $\lambda/\Delta\lambda=10\ 000$. The spatial resolution of the spectrometer was better than 50 μm. The argon plasma emission spectra were recorded in the fifth order of crystal reflection for the spectral region $\lambda=3.25$–3.45 Å. The typical spectrum obtained is presented in Fig. 1(b). It can be seen from this figure that the heliumlike Ar ions emit only from a small spatial region with dimensions less than 300 μm in both directions and do not radiate during the plasma expansion. This results in the small spectral widths of the observed lines and makes it possible to measure the wavelengths with a very good accuracy. A big advantage of using the gas-puff target is to avoid the large hydrodynamic motions associated with the expansion of solid targets. As a result, we have smaller ion temperatures and narrower linewidths with the gas-puff target in the region of interest.

A measurement of the $K\beta$ emission of heliumlike Ar is shown in Fig. 2. For the wavelength measurement we used the spectrometer dispersion curve calculated by the ray-tracing code. Two lines, $1s3p\ ^1P_1$–$1s^2\ ^1S_0(K\beta_1)$, and the satellite line designated by the number 9 in Table I and Fig. 2 were used as reference lines to avoid the uncertainties connected with the absolute line positions on the film and with the distance between the crystal and the plasma. The wavelengths of these reference lines were obtained from Ref. [3]. The absolute accuracy of our wavelength measurements is defined mainly by the accuracy of the reference lines and is better than 0.2 mÅ for lines observed in the same order of reflection as the reference lines. For lines observed in the first order of reflection ($5d$-$2p$ transitions in lithiumlike Ar) the accuracy is limited by the uncertainty in the ratio d_5/d_1 of the interplanar spacing of the mica crystal in the fifth and first orders of reflections and according to our estimation is about 3 mÅ. The results obtained are presented in Table I.

We have used the quasistationary collision-radiative kinetic model to describe the emission spectrum in the vicinity of the $K\beta_1$ line. This model was based on atomic data for $1s2l3l'$ and $1s3l3l'$ lithiumlike and $1s2l2l'3l''$ berylliumlike satellites calculated by the HULLAC set of atomic physics codes, which calculate wave functions, energy levels, and radiative transition rates by the relativistic, multiconfiguration parametric potential method with full configuration interaction [6]. The collisional excitation rates were calculated in the distorted-wave approximation; an efficient technique, which performs an angular factorization of both direct and exchange contributions to the excitation cross sections and interpolates the necessary radial integrals as a function of the threshold energy used [7]. The autoionization rates were obtained from a factorization-interpolation technique using a single consistent potential for the bound and continuum orbitals [8]. In the collisional-radiative kinetic model all states belonging to the $1s2l3l'$, $1s3l3l'$, and $1s2l2l'3l''$ configurations were taken into account as individual levels. Note that the same model was used in Ref. [3] to describe the argon spectra in the tokamak. For singly excited heliumlike Ar levels we used the simpler kinetic model [9] with excitation cross sections calculated in Ref. [10]. In the synthetic spectra each line was modeled by a Gaussian-shaped curve with a width that equals the width of the $K\beta_1$ line as observed in the experiment. The result of the spectral modeling is presented in Fig. 3 together with the experimental data obtained in the present work. For comparison, the analogous spectrum observed in the tokamak [3] is shown in Fig. 4. It can be seen from Figs. 3 and 4 that the atomic model used describes adequately both the dense ($N_e=10^{21}$ cm^{-3}) and the rarefied ($N_e=10^{13}$ cm^{-3}) plasma except for a discrepancy of a factor of 2 for the $K\beta_2$ line in the tokamak plasma, as noticed in Ref. [3], which used a slightly different model for the excitation rates for the singly excited heliumlike ions.

It is interesting to compare the spectra emitted by the tokamak and laser-produced plasma. Looking at Fig. 4, we note that in the tokamak plasma the $K\beta_1$ line is the dominant spectral feature, and features formed by the lithiumlike and berylliumlike satellites are one or two orders of magnitude smaller in intensity, while in the laser-produced plasma (Fig. 3) the intensities of the $K\beta_1$ line and the lithiumlike satellites are approximately equal. This difference, of course, is explained by the differences in the plasma temperatures: the electron temperature $T_e=2.3$ keV in the tokamak and $T_e=620$ eV in the laser-produced plasma. We also see from Fig. 4 that a different set of lines can be observed in tokamak and laser-produced plasma. For example, some satellites from the $1s3l3l'$ and $1s2l2l'3l''$ levels of lithiumlike and berylliumlike Ar ions were observed from the tokamak plasma and are absent in the spectrum of the laser-produced plasma and, vice versa, satellites marked by numbers 11–15 are present in the second case (Fig. 3) and are not observed in the first one (Fig. 4). These differences are connected mainly with the electron plasma density. A very interesting situation is realized for the spectral feature marked by number 8 in Fig. 3. In the laser-produced plasma, this feature is formed by the $(1s2p_{3/2}3p_{3/2})_{J=5/2}$-$(1s^22p)_{J=3/2}$ transition (see Table I) and has wavelength $\lambda=3.4187$ Å. In the tokamak spectra, a feature with a very similar wavelength $\lambda=3.4193$ Å was observed, but in this case it is the $(1s2p_{3/2}3p_{3/2})_{J=1/2}$-$(1s^22p)_{J=1/2}$ transition. It should be noted that for lines observed in both the tokamak and the laser-produced plasma the wavelength measurements give

TABLE I. Wavelengths of the radiative transitions in heliumlike and lithiumlike Ar ions. The reference lines 5 and 9 used in the present measurement are marked with an asterisk. The uncertainty in the last digit is given in parenthesis. The reference for the various wavelengths are given as footnotes. The transition is described using *jj* coupling with the total angular momentum *J* given as a subscript after the parenthesis.

		λ_{expt} (Å)		λ_{theor} (Å)			
Key	Transition	laser plasma	tokamak	present	a–d	e–g	h,i
1	$(1s2s4p_{3/2})_{1/2}$-$(1s^22s)_{1/2}$				3.2599[a]	3.2611[e]	3.2622[h]
1	$(1s2s4p_{3/2})_{3/2}$-$(1s^22s)_{1/2}$	3.2606(4)	3.2616[a]		3.2600[a]	3.2612[e]	3.2623[h]
1	$(1s2p_{3/2}4p_{3/2})_{5/2}$-$(1s^22p)_{3/2}$				3.2600[a]	3.2605[e]	3.2623[h]
2	$(1s2p_{3/2}4p_{3/2})_{5/2}$-$(1s^22p)_{3/2}$	3.2708(4)	3.2708[a]		3.2699[a]	3.2704[e]	3.2722[h]
2	$(1s2p_{1/2}4p_{3/2})_{3/2}$-$(1s^22p)_{1/2}$				3.2697[a]	3.2707[e]	3.2724[h]
3	$(1s^25d)_{3/2}$-$(1s^22p)_{1/2}$	16.593(3)			16.5968[c]	16.5962[f]	
4	$(1s^25d)_{5/2}$-$(1s^22p)_{3/2}$	16.662(3)			16.6666[c]	16.6655[f]	
5	$1s3p\ ^1P_1$–$1s^2\ ^1S_0$	3.3655*	3.3655[b]		3.3658[d]	3.3653[g]	3.3656[i]
6	$1s3p\ ^3P_1$–$1s^2\ ^1S_0$	3.3695(2)	3.3696[b]		3.3698[d]	3.3700[g]	3.3696[i]
7	$(1s2s3p_{3/2})_{3/2}$-$(1s^22s)_{1/2}$	3.4059(2)	3.4059[b]	3.4052	3.4059[d]		3.4056[h]
7	$(1s2s3p_{1/2})_{1/2}$-$(1s^22s)_{1/2}$			3.4061			3.4065[h]
8	$(1s2p_{3/2}3p_{3/2})_{3/2}$-$(1s^22p)_{3/2}$			3.4179	3.4185[d]		3.4186[h]
8	$(1s2p_{3/2}3p_{3/2})_{5/2}$-$(1s^22p)_{3/2}$	3.4187(2)		3.4190	3.4194[d]		3.4194[h]
8	$(1s2p_{3/2}3p_{1/2})_{3/2}$-$(1s^22p)_{3/2}$			3.4192	3.4195[d]		3.4198[h]
9	$(1s2s3p_{3/2})_{1/2}$-$(1s^22s)_{1/2}$			3.4221	3.4231[d]		3.4224[h]
9	$(1s2s3p_{3/2})_{3/2}$-$(1s^22s)_{1/2}$	3.4225*	3.4225[b]	3.4222	3.4232[d]		3.4226[h]
10	$(1s2p_{3/2}3p_{3/2})_{3/2}$-$(1s^22p)_{1/2}$			3.4270	3.4271[d]		3.4270[h]
10	$(1s2p_{3/2}3p_{3/2})_{5/2}$-$(1s^22p)_{3/2}$	3.4276(2)		3.4276	3.4278[d]		3.4280[h]
11	$(1s2p_{3/2}3p_{3/2})_{3/2}$-$(1s^22p)_{3/2}$	3.4302(2)		3.4299	3.4301[d]		3.4299[h]
12	$(1s2p_{1/2}3p_{3/2})_{1/2}$-$(1s^22p)_{1/2}$			3.4337			3.4334[h]
12	$(1s2p_{1/2}3p_{3/2})_{3/2}$-$(1s^22p)_{1/2}$	3.4327(2)		3.4341			3.4337[h]
12	$(1s2p_{1/2}3p_{3/2})_{3/2}$-$(1s^22p)_{3/2}$			3.4344			3.4342[h]
13	$(1s2p_{1/2}3p_{3/2})_{3/2}$-$(1s^22p)_{3/2}$	3.4360(2)		3.4370	3.4365[d]		3.4367[h]
14	$(1s2s3d_{5/2})_{3/2}$-$(1s^22p)_{1/2}$	3.4427(2)		3.4435	3.4438[d]		3.4434[h]
15	$(1s2s3d_{5/2})_{3/2}$-$(1s^22p)_{1/2}$	3.4469(2)		3.4465	3.4468[d]		3.4465[h]

[a]Reference [20].
[b]Reference [3].
[c]Reference [12].
[d]Reference [13].
[e]Reference [19].
[f]Reference [11].
[g]Reference [15].
[h]References [16–18].
[i]Reference [14].

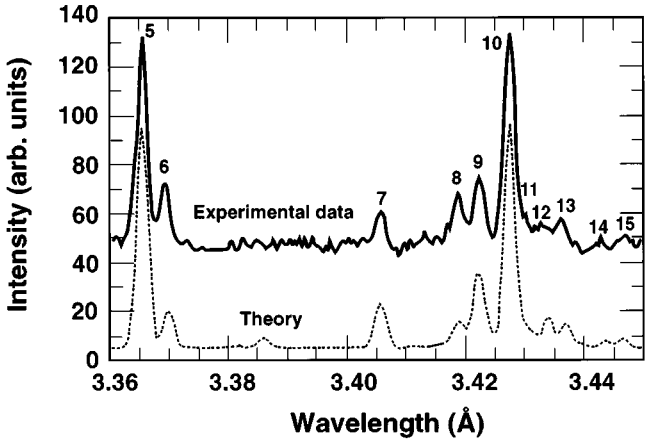

FIG. 3. Comparison of the experimental and theoretical spectra for the Ar-gas-puff laser-produced plasma.

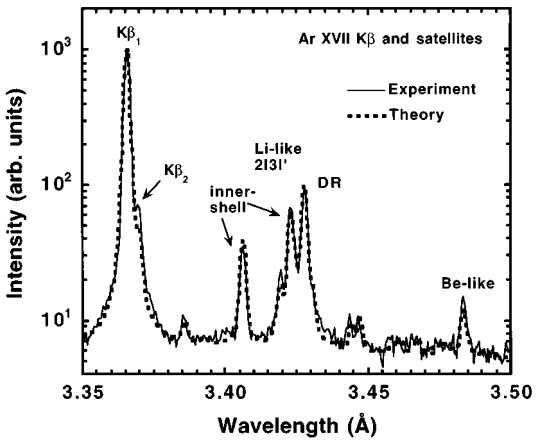

FIG. 4. Comparison of the experimental and theoretical spectra for the Ar tokamak plasma.

practically the same result (see Table I). Because the satellite spectrum is sensitive both to the electron plasma temperature and the density, the comparison of the experimental data with the theoretical one enables us to determine the plasma parameters. For example, for the case of the laser-produced plasma, this method gives $N_e=10^{21}$ cm^{-3} and $T_e=620$ eV for the plasma region where the heliumlike Ar emission occurs.

In Table I we compare our wavelength measurements and current calculations with other experiments and theoretical results. For the lithiumlike ions the semiempirical method [11] and Z expansion method (MZ code) [12] are used. Several references are included for the heliumlike $K\beta$ lines [13–15]. For the lithiumlike satellites, the Z expansion method [13], the multiconfiguration Dirac-Fock method [16–18], the Hartree-Fock method [19], and the Thomas-Fermi-Dirac method [20] are all compared. The published wavelengths calculated with the multiconfiguration Dirac-Fock method using the YODA code [16] have had the energy of the transitions shifted by adding 15 230 cm^{-1} for the $n=4$ lines and 16 587 cm^{-1} for the $n=3$ satellite lines in Table I. This shift is described in Refs. [17,18] and is used to shift the heliumlike $K\beta$ and $K\gamma$ lines to the correct wavelength. There is good agreement among the methods to less than 1-mÅ level, but the best agreement between experiment and theory varies line by line. Some of the biggest differences in the theory are for line 9, where the theory varies by as much as 1 mÅ. The biggest difference between the experiment and theory is for line 12, where the difference is slightly more than 1 mÅ. While such differences appear small, they are in fact very important for proper modeling of experimental spectra, especially in cases where several lines blend and the shape of a given feature critically depends on accurate knowledge of the individual line positions.

In the present paper $K\beta$ heliumlike Ar emission spectra have been investigated for the case of high-density laser-produced plasma. The positions of the $1s2l3l'$-$1s^22l$, $1s2l4l'$-$1s^22l$, and $K\beta_2$ lines have been measured with a very high accuracy of 0.2 mÅ and some satellite transitions were observed and identified. The comparison of the measured argon spectrum with the theoretical data have allowed us to determine the gas-puff laser-produced plasma parameters. It should be noted that only by using different kinds of plasma sources is it possible to obtain the most complete information on the ionic spectra. In particular, data obtained in the present work together with the data obtained in the experiments on the tokamak [3] and EBIT [4] facilities gives a detailed picture of Ar-ion emission in the vicinity of the $K\beta_1$ line of heliumlike Ar.

We would like to thank NATO for support under the High Technology Collaborative Research Grant No. 950396. The work was supported, in part, by the State Committee for Scientific Research of Poland in the frame of the KBN, Grant No. 2 P02B 013 11. The work of P.B., J.N., and A.L.O. was performed under the auspices of the U.S. Department of Energy by the Lawrence Livermore National Laboratory under Contract No. W-7405-ENG-48.

[1] K. W. Hill, P. Beiersdorfer, M. Bitter, E. Fredrickson, S. von Goeler, H. Hsuan, K. McGuire, N. R. Sauthoff, S. Sesnic, and J. E. Stevens, in *Course and Workshop on Basic and Advanced Diagnostic Techniques for Fusion Plasmas, Varenna, 1986*, edited by P. Stott *et al.* (Office for Official Publications of the European Communities, Luxemborg, 1987), Vol. I, p. 169.

[2] V. A. Boiko, V. G. Palchikov, I. Yu. Skobelev, and A. Ya. Faenov, *X-Ray Spectroscopy of Multicharged Ions* (Energoatomizdat, Moscow, 1988).

[3] P. Beiersdorfer, A. L. Osterheld, T. W. Phillips, M. Bitter, K. W. Hill, and S. von Goeler, Phys. Rev. E **52**, 1980 (1995).

[4] A. J. Smith, P. Beiersdorfer, V. Decaux, K. Widmann, K. J. Reed, and M. H. Chen, Phys. Rev. A **54**, 462 (1996).

[5] J. Nilsen, P. Beiersdorfer, S. R. Elliott, T. W. Phillips, B. A. Bryunetkin, V. M. Dyakin, T. A. Pikuz, A. Ya. Faenov, S. A. Pikuz, S. von Goeler, M. Bitter, P. A. Loboda, V. A. Lykov, and V. Yu. Politov, Phys. Rev. A **50**, 2143 (1994).

[6] M. Klapisch, Comput. Phys. Commun. **2**, 239 (1971); M. Klapisch, J. L. Schwob, B. S. Fraenkel, and J. Oreg, J. Opt. Soc. Am. **61**, 148 (1977).

[7] A. Bar-Shalom, M. Klapisch, and J. Oreg, Phys. Rev. A **38**, 1773 (1988).

[8] J. Oreg, A. Bar-Shalom, W. H. Goldstein, and M. Klapisch, Phys. Rev. A **44**, 1750 (1991).

[9] V. A. Boiko, A. V. Vinogradov, S. A. Pikuz, I. Yu. Skobelev, A. Ya. Faenov, and E. A. Yukov, J. Phys. B **10**, 3387 (1977).

[10] L. A. Vainshtein, I. I. Sobelman, and E. A. Yukov, *Excitation of Atoms and Broadening of Spectral Lines* (Nauka, Moscow, 1979).

[11] B. Édlen, Phys. Scr. **19**, 255 (1979).

[12] L. A. Vainshtein and U. I. Safronova (private communication).

[13] U. I. Safronova, M. S. Safronova, R. Bruch, and L. A. Vainshtein, Phys. Scr. **51**, 471 (1995).

[14] J. Nilsen, J. H. Scofield, and E. A. Chandler, Appl. Opt. **31**, 4950 (1992).

[15] V. A. Boiko, V. G. Palchikov, I. Yu. Skobelev, and A. Ya. Faenov, *Spectroscopic Constants of Atoms and Ions: Spectra of Atoms with One and Two Electrons* (CRC, Boca Raton, FL, 1994).

[16] J. Nilsen, At. Data Nucl. Data Tables **38**, 339 (1988).

[17] J. Nilsen and U. I. Safronova, J. Quant. Spectrosc. Radiat. Transfer **49**, 371 (1993).

[18] U. I. Safronova and J. Nilsen, J. Quant. Spectrosc. Radiat. Transfer **51**, 853 (1994).

[19] C. P. Bhalla and T. W. Tunnell, J. Quant. Spectrosc. Radiat. Transfer **32**, 141 (1984).

[20] E. Källne, J. Källne, J. Dubau, E. S. Marmar, and J. E. Rice, Phys. Rev. A **38**, 2056 (1988).